Earth Planet. Sci. Lett. 646 (2024) 118999



Contents lists available at ScienceDirect

Earth and Planetary Science Letters

journal homepage: www.elsevier.com/locate/epsl



Anomalously high relief on Denali, Alaska, caused by tectonic, lithologic, and climatic drivers

A. Matmon [a,*], P.J. Haeussler [b], M. Loso [c], ASTER Team [d,1]

[a] Institute of Earth Sciences, Hebrew university of Jerusalem, Jerusalem, Israel
[b] U.S. Geological Survey, Anchorage, AK 99508, USA
[c] National Park Service, Copper Center, AK 99573, USA
[d] Centre de Recherche et d'Enseignement de Geosciences de l'Environnement (CEREGE), Technopôle de l'Arbois, BP80, 13545 Aix-en-Provence, France

ARTICLE INFO

Editor: J.P. Avouac

Keywords:
Relief increase
Mt. Denali
Cosmogenic isotopes
Erosion rates

ABSTRACT

We assess the growth of anomalously high relief on Denali, located in the Alaska Range, Alaska, and the tallest mountain in North America (6190 masl). Denali is 3000 m taller than most surrounding peaks. It lies inside a 19° restraining bend in the active Denali fault system that is moving at about 7 mm/yr, providing a tectonic and structural driver for ongoing rock uplift. High relief around Denali is also due, in part, to its granitic rock type and low fracture density relative to adjacent metasediments. Here we show that unique climatic conditions at high elevations also contribute to the growth of relief. We examine ^{10}Be concentrations in 1) three new gravel samples between 3500 and 5200 m elevation from sites unaffected by recent glacial erosion, 2) previously published samples from a sidewall of the Kahiltna Glacier from 2400 to 2800 masl, 3) previously published data for samples collected from medial moraines along the length of the Kahiltna Glacier from ~500 to 1400 masl, and 4) previously published data for alluvial samples collected along the Kahiltna River at an elevation of ~200 masl. These samples constitute a transect extending >5000 vertical meters, and the data establish that erosion rates decrease with elevation and contribute to the growth of relief. Erosion rates for the three new high-elevation samples are calculated to 4.6 ± 0.6 mm/ka at 5200 masl, 28.6 ± 3.7 mm/ka at 4000 masl, and 38 ±5 mm/ka at 3500 masl. Erosion rates at intermediate elevations, on the sidewall of the Kahiltna Glacier, range between 160 and 327 mm/ka. Along the medial moraines inferred erosion rates range between 140 and 537 mm/ka, and basin-wide erosion rates calculated from sediments in the river below the glacier range between 450 and 896 mm/ka. These differences in erosion rates can create relief of 3 km within 1–10 Ma, well within the estimated period of increase in rock uplift and exhumation on Denali over the last ~6 Ma. Meteorological data from 2130 to 5550 masl at 5 sites show temperatures rarely exceed freezing above 4000 masl elevation, indicating that frost weathering currently plays a diminished role in erosion at high elevations. The immediate implication of this temperature and erosional correlation is an increase in relief. This is the first study to directly measure a significant decrease in erosion rates at high elevations in the relative absence of frost weathering. The results highlight the combined influence of rock type, glacial erosion, and permanent sub-zero temperatures on erosion rates. In combination with active faulting, the data explain the resultant increase in relief along the southern side of the Alaska Range over the past 100 ka.

1. Introduction

The idea that erosion enhances growth of relief caused by tectonics, and the quantification of such growth have been subjects of many studies (e.g., Whittaker, 2012; Hurst et al., 2013a; Small and Anderson, 1998). The growth of extraordinary relief, for example, in the Himalayan syntaxes, has been ascribed to the interplay between tectonics and erosion (e.g. Zeitler et al. 2001). Moreover, climate, manifested by glacial erosion, may be a major factor in promoting or limiting growth of relief in some settings (Brozović et al., 1997; Whipple et al., 1999; Mitchell and Montgomery, 2006; Brockelhurst et al., 2008; Lease, 2018). Rock-type variations are also recognized as a cause for major

* Corresponding author.
E-mail address: arimatmon@mail.huji.ac.il (A. Matmon).
[1] ASTER Team: M. Arnold, G. Aumatre, and K. Keddadouche.

https://doi.org/10.1016/j.epsl.2024.118999
Received 30 January 2024; Received in revised form 18 August 2024; Accepted 4 September 2024
Available online 13 September 2024
0012-821X/© 2024 Elsevier B.V. All rights are reserved, including those for text and data mining, AI training, and similar technologies.

changes in relief. The roles of rock type and strength have been demonstrated in landscapes in which contrasting rock types are adjacent to each other (Dethier et al., 2014; Ward et al., 2012). The change in relief is examined by comparing the erosion of summits with the erosion of adjacent intermountain valleys (Quigley et al., 2007) as well as through modelling that considers erosion, tectonic uplift and isostatic response to unloading (e.g., Avouac and Burov, 1996). The increasing use of cosmogenic isotopes in geomorphological studies and the ability to quantify rates of erosion with increasing accuracy, enable the quantification of the growth or reduction of relief over various spatial scales (from the scale of channel-ridge couplets to the mountain ranges) and temporal scales (10^2–10^6 years).

Portenga and Bierman (2011) showed that slope gradient is a major factor affecting erosion rates. Therefore, the increase of relief in terrains where summits are flat and adjacent slopes are steep. This difference is seen in both tectonically active (e.g. western North America mountain ranges) and inactive (e.g. Appalachians) mountain ranges and is expressed by at least an order of magnitude difference in average erosion rates measured on mountain tops relative to basin-wide erosion rates (e.g. Matmon et al., 2003; Riebe et al., 2003). Several studies demonstrated the growth of relief due to incision alone (Quigley et al., 2007; Small, 1995; Small and Anderson, 1998; Hancock and Kirwan, 2007). Incision removes mass and thus promotes isostatic uplift of the entire mountain range. However, while erosion on mountain tops is slow, river bottoms are incised rapidly such that river-bottom uplift is nearly negated by intense incision. This difference results in the growth of relief.

An additional factor affecting the development of relief is elevation. Where mountain range summits are in extremely cold conditions, which inhibit erosion, while lower slopes have freeze-thaw cycles that promote erosion, differential erosion will develop and lead to an increase in relief (Griffiths, 1952; Lave et al., 2023). Furthermore, the introduction of alpine glaciers into an unglaciated mountain range during a transition from interglacial to glacial periods, would amplify this process of relief growth (Montgomery, 1994; Small, 1995; Small et al., 1997; Small and Anderson, 1998; Whipple et al., 1999; Brocklehurst and Whipple, 2002). Mountain tops above alpine cirques are mostly unaffected by glacial erosion and constantly frozen; however, the terrain downstream of glacial cirques is intensely eroded and thus relief grows substantially.

The concept that erosion rates decrease with increasing elevation (and decreasing temperatures) in glacier-covered terrain has been around for several decades. However, this concept has been best developed for glaciers where erosion rates are controlled by sliding velocity (Boulton, 1974; Herman et al., 2015), entrained debris within the glacier (Hallet, 1981), and thermal structure of the glacier base (Boulton, 1972). We also note the underappreciated work of Griffiths (1952) on the Denali massif, Alaska, in which he noted: *"The erosional process above 16,500 feet appears to be more akin to the process under severe polar conditions than to the type of glacial geomorphic process displayed by mountain masses in more temperate climates or at lower elevation…"* He continued, *"Above the 16,500-foot level, the weathering and erosion processes seem to be highly modified and greatly retarded by the climatic characteristics of the mountain…"*. Griffiths (1952) also noted the role of rock type differences and glacial scouring below cirques (as opposed to no scouring above the cirques) in creating an erosional gradient with elevation and producing relief. This insight into the development of topography was at least several decades ahead of its time, yet the basic concepts have proven challenging to demonstrate.

The study we present here is the first we are aware of to have direct measurements of erosion rate and temperature on a single mountain that transitions from lower altitudes, where frost cracking acts to increase erosion and reduce topography, to high elevations that are perpetually below freezing and where erosion rates become very low. In this study, we use new and previously published ^{10}Be concentrations (Matmon et al., 2020) measured in several types of samples to determine erosion rates (e.g. Bierman, 1994). We combine the cosmogenic isotope data with high-altitude meteorological data to understand the effects of elevation and temperature on erosion and, by inference, on the production of relief. The samples are from the Kahiltna drainage basin, Alaska Range, Alaska, that drains the southwestern aspect of Denali, the tallest mountain (6190 m) on the North American continent. The ^{10}Be samples come from: 1) granitic bedrock samples collected from flat bedrock surfaces, above glacial cirques, at elevations between 3500 and 5200 masl, 2) granitic bedrock samples collected from cirque sidewalls at an elevation range between 2400 and 2800 masl, from the of the Kahiltna Glacier tributaries, 3) medial moraines along the length of the Kahiltna Glacier, from ~500 to 1400 masl, and 4) alluvial samples collected from along the Kahiltna River at an elevation of ~200 masl. The results highlight the combined influence of rock type, glacial erosion, and permanent sub-zero temperatures on erosion rates and indicate the resultant increase in relief along the southern side of the Alaska Range at least over the last 100 ka.

1.1. Geographic, topographic and geologic setting

Denali lies in the central Alaska Range of southern Alaska (Fig. 1). The Alaska Range parallels the trace of the active dextral Denali fault, which now accommodates far-field deformation related to the collision of the Yakutat microplate into the southern Alaska margin (e.g. Haeussler, 2008; Eberhart-Phillips et al., 2003). As Denali lies adjacent to a restraining bend in the Denali fault system, the high topography is a product of movement of material through the bend (Plafker et al., 1992; Fitzgerald et al., 1993; Haeussler, 2008; Lease et al., 2016; Burkett et al., 2016; Benowitz et al., 2021). The Denali fault slip rate in this region is 7 mm/yr (Haeussler et al., 2017a), and this results in a long-term rock uplift rate of Denali of about 1.5 mm/yr since about 6 Ma (Fitzgerald et al., 1995).

The Kahiltna drainage system (~15,000 km^2 area upstream of our lowest elevation samples) drains the southern face of the Denali massif (Fig. 2). The head of the Kahiltna catchment is at the summit of Denali, and extends 75 km south along the Kahiltna Glacier, the longest valley glacier on the south side of the Alaska Range. The ELA (equilibrium line altitude) of the Kahiltna Glacier is about 1875 masl (Goodwin et al. 2012). This glacier feeds the braided Kahiltna River, which travels about 80 km, to its junction with the Susitna River, which then drains into the ocean in Cook Inlet.

The Denali massif consists of granodiorite that intruded previously deformed and slightly metamorphosed Cretaceous flysch 58 Ma (Reed and Nelson, 1980; Hung, 2008; Hampton et al., 2010). The bedrock underlying the high topography of Denali is almost entirely within this granodiorite, with the exception of some flysch on the north summit (5934 masl, or 19,470 ft). West of the upper Kahiltna Glacier are an assortment of moderately metamorphosed Paleozoic sediments and volcanic rocks, which were intruded by granodiorite of the Foraker pluton about 38 Ma (Reed and Lanphere, 1973; Reed and Nelson, 1980; Regan et al. 2020). Thus, the geology of the Kahiltna drainage is dominated by two rock types – granitic rocks and slate/greywacke turbidites (Reed and Nelson, 1980; Fig. 2). The granitoids dominate the high topography and all summits are underlain by granitoids. Easily erodible and fractured dark-colored rock types (slate and greywacke) compose the lower slopes south of the high-elevation mountain summits.

2. Methods

For this study, three new high-elevation samples were collected from the southwest side of Denali for cosmogenic ^{10}Be analysis (Figs. 2, 3 and Table 1). These samples were composed of >100 angular and fresh clasts (up to 3 cm) that were collected from relatively flat, but narrow, granitic bedrock surfaces that are perpetually windswept with little snow accumulation, at elevations of 3535, 4023, and 5242 masl. We interpret the ^{10}Be concentrations measured in these samples as indicating steady-state erosion of the underlying bedrock surfaces. These three new

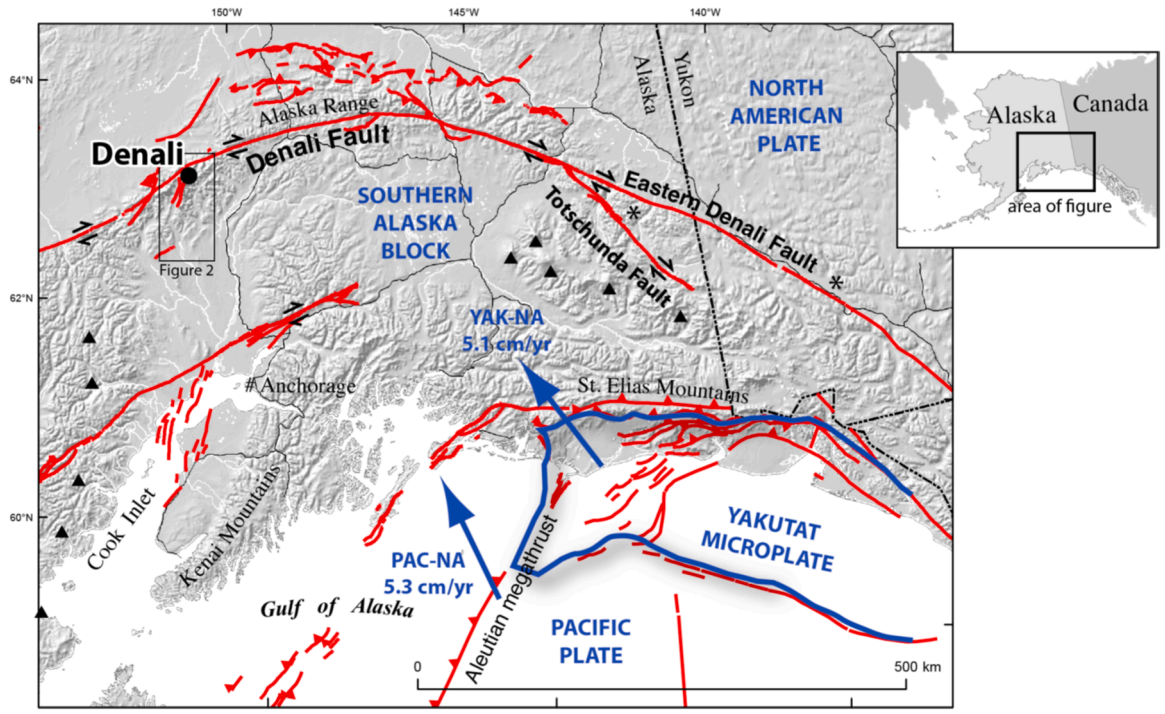


Fig. 1. A. General location map indicating the location of Denali, and the major tectonic feature including the bend in the Denali fault. YAK-NA – Yakutat-north America, PAC—NA – Pacific-north America. Slip rates from Haeussler (2008) and Eberhart-Phillips et al. (2003).

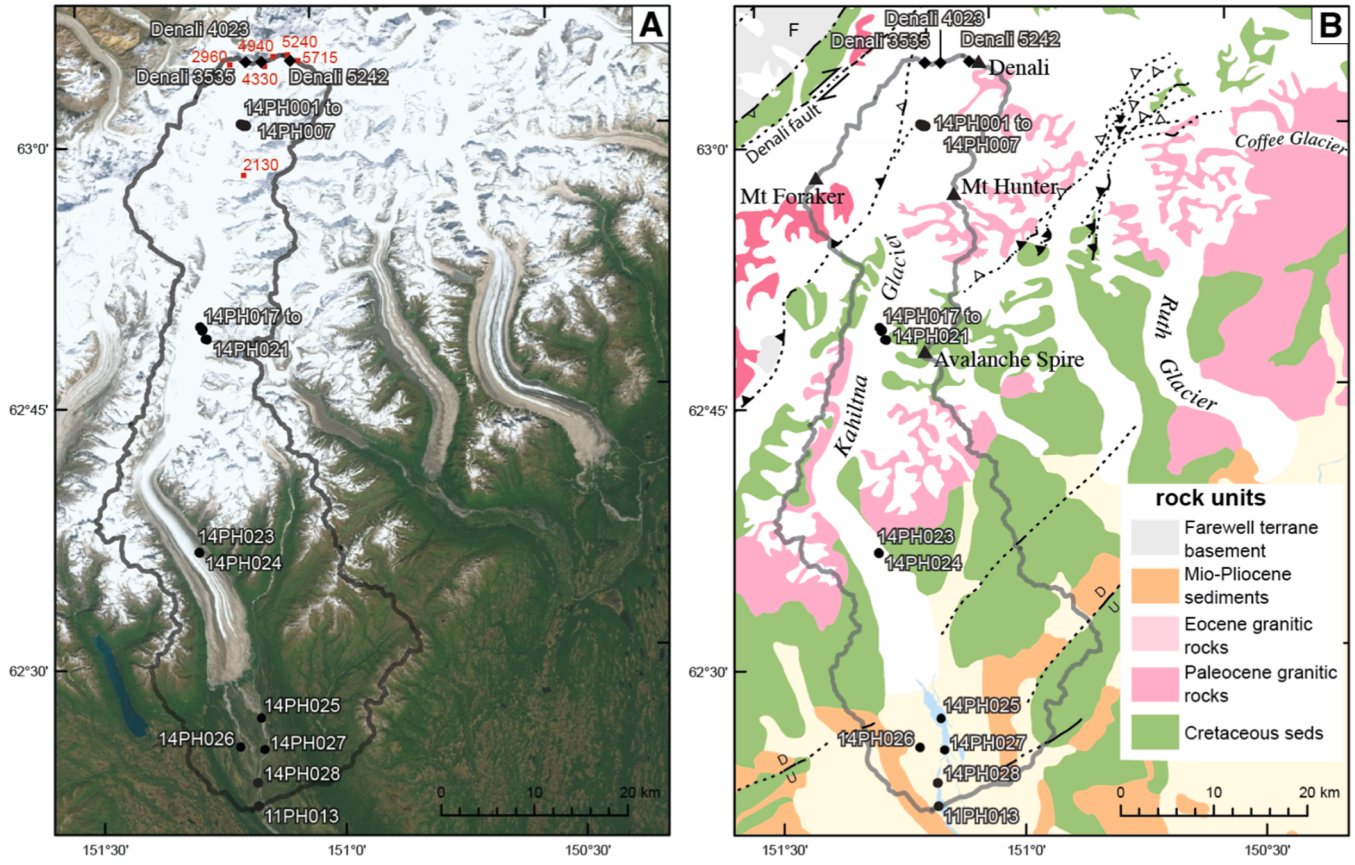


Fig. 2. A. Close-up on the Kahiltna drainage basin. Samples from Matmon et al. (2020) are indicated by black dots and sample name. High elevation samples are indicated by solid black diamonds. Weather station locations are indicated with red solid squares with elevations in red text. B. Close-up on the Kahiltna drainage basin indicating lithologic distribution throughout the basin. Samples from Matmon et al. (2020) are indicated by black dots and sample name. High elevation samples are indicated by solid diamonds.

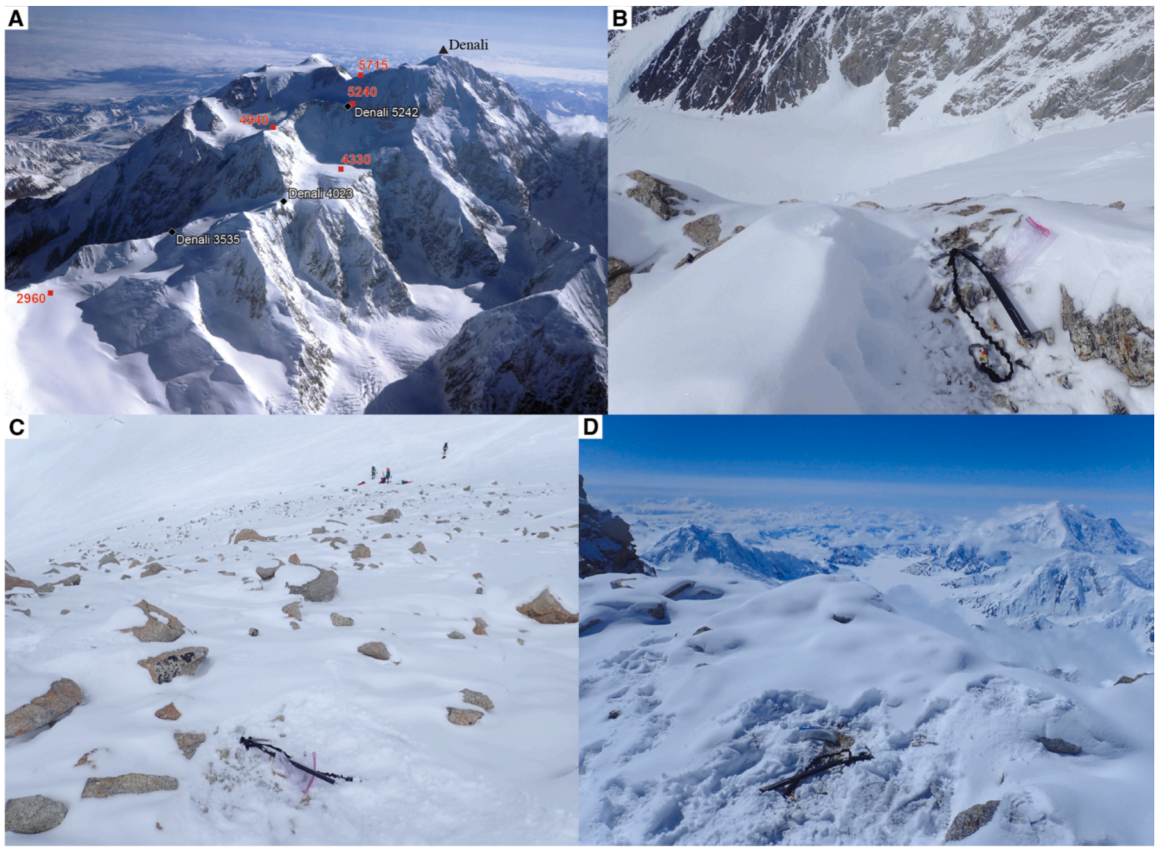


Fig. 3. Locations and photos of high elevation samples. A) High elevation samples are indicated by solid diamonds. Numbers in sample name indicate elevation in meters above sea level. Weather station locations are indicated with red solid squares. Numbers next to station location indicate elevation in meters above sea level. B-D. Specific sampling sites. Notice the thin snow cover, the result of constant windy conditions.

Table 1
Field data for Kahiltna basin samples.

Sample Name	N Lat (°)	Long (°)	Sample Elevation (masl)	Geomorphic location	Geographic location	Distance downstream from glacier terminus (km)	Sample composition
Denali5242	63.079	−151.055	5242	Bedrock flat	High Denali slopes		granite
Denali4023	63.067	−151.109	4023	Bedrock flat	High Denali slopes		granite
Denali3535	63.076	−151.135	3535	Bedrock flat	High Denali slopes		granite
14PH001	63.016	−151.146	2855	Cirque cliff	Kahiltna Peaks		granite
14PH002	63.015	−151.146	2797	Cirque cliff	Kahiltna Peaks		granite
14PH003	63.015	−151.147	2734	Cirque cliff	Kahiltna Peaks		granite
14PH004	63.016	−151.149	2678	Cirque cliff	Kahiltna Peaks		granite
14PH005	63.016	−151.151	2594	Cirque cliff	Kahiltna Peaks		granite
14PH006	63.016	−151.153	2486	Cirque cliff	Kahiltna Peaks		granite
14PH007	63.017	−151.156	2407	Cirque cliff	Kahiltna Peaks		granite
14PH017A	62.820	−151.257	1390	Medial moraine	Kahiltna Glacier		granite and flysch
14PH018A	62.824	−151.260	1394	Medial moraine	Kahiltna Glacier		granite
14PH019A	62.821	−151.255	1392	Medial moraine	Kahiltna Glacier		granite and flysch
14PH020A	62.812	−151.249	1369	Medial moraine	Kahiltna Glacier		flysch and granite
14PH021A	62.812	−151.247	1377	Medial moraine	Kahiltna Glacier		flysch
14PH023A	62.608	−151.282	551	Medial moraine	Kahiltna Glacier		granite
14PH024A	62.608	−151.281	559	Medial moraine	Kahiltna Glacier		granite
14PH025	62.447	−151.166	212	river	Kahiltna River	5	sand
14PH026	62.420	−151.212	213	river	Kahiltna River	7	sand
14PH027	62.417	−151.161	213	river	Kahiltna River	8	sand
14PH028	62.385	−151.178	217	river	Kahiltna River	11	sand
11PH013	62.363	−151.180	214	river	Kahiltna River	14	sand

samples were combined with previously collected and analyzed samples (Matmon et al., 2020; Fig. 2) to form a 5000-meter elevation profile:

a. Seven samples of mixed clasts collected from bedrock ledges that range in elevation between 2407 and 2855 masl, above the ELA of the Kahiltna Glacier (samples 14PH001 to 14PH007 in Matmon et al., 2020; Fig. 2 and Table 1). The samples lie on the southwestern flank of a granitic mountain along the east side of the upper Kahiltna Glacier. The ^{10}Be concentrations measured in these samples were interpreted by Matmon et al. (2020) as indicating bedrock erosion of the adjacent bedrock ledges.

b. Seven samples of amalgamated clasts collected from medial moraines on the middle to lower Kahiltna Glacier west and south of Avalanche Spire, below the ELA. Five samples were collected from elevations ranging between 1377 and 1390 masl (samples 14PH017 to 14PH021 in Matmon et al., 2020; Fig. 2 and Table 1) and two samples were collected at elevations of 551 and 559 masl (14PH023 and 14PH024 in Matmon et al., 2020; Fig. 2). Matmon et al. (2020) interpreted ^{10}Be concentrations measured in these samples as indicating steady-state bedrock erosion of the slopes adjacent to the sampled moraines.
c. Five sediment samples were collected from the Kahiltna River downstream from the glacier terminus (samples 14PH025 to 14PH028 and sample 11PH013; Fig. 2 and Table 1). These samples were collected at an elevation of ~200 masl and enable us to roughly evaluate the rate at which slopes adjacent to the sample locations are eroding.

Samples were prepared for ^{10}Be analysis at the Cosmogenic Laboratory of The Hebrew University of Jerusalem following standard procedures (Matmon et al., 2020; Kohl and Nishiizumi, 1992; Bierman and Caffee, 2001). All samples were analyzed for their ^{10}Be/^{9}Be ratios at the accelerator mass spectrometry (AMS) facility (ASTER) at Cerege, Aix-en-Provence, France. Samples were normalized against standard BeO STD-11 with an average ^{10}Be/^{9}Be ratio of 6.00353×10^{-12}.

To provide estimates of discrete bedrock location and slope erosion rates we consider the measured concentrations as representing steady-state erosion rates following Lal (1991) and assuming $t >> 1/(\lambda+\mu\varepsilon)$:

$$\varepsilon = \frac{1}{\mu(P/N - \lambda)} \quad (1)$$

where P is the production rate (atoms g^{-1} yr^{-1}), N is the measured concentration (atoms g^{-1}), μ is the absorption coefficient (cm^{-1}), which is equal to ρ/Λ with ρ being the target's density (g cm^{-3}) and Λ the attenuation length (g cm^{-2}), ε is the erosion rate, and λ is the decay constant of the measured nuclide. A sea level high latitude spallation production rate of 4.01 atoms g^{-1} SiO_2 yr^{-1} (Borchers et al., 2016) was used for all calculations. Production rates were scaled for latitude and altitude following Stone (2000). Muon production values and attenuation lengths are from Granger and Muzikar (2001) and Granger and Smith (2000). A neutron attenuation length of 165 g cm^{-2} and ^{10}Be decay constant of 4.99×10^{-7} yr^{-1} were used for all calculations (Balco et al., 2008). We applied a rock density of 2.65 g cm^{-3}. Topographic shielding corrections were applied only to the seven samples collected from the Kahiltna Peaks along the upper part of the Kahiltna Glacier cirque (Matmon et al., 2020). All new and previously studied sample sites are windswept and we did not see evidence for significant long-term accumulation of snow. Furthermore, there is significantly less snowfall at high elevation than at more moderate elevations, contributing to the paucity of snow cover and glacier cover at higher elevations (Loso, 2022). At the time of sample collection, high elevation sampling sites (>3500 masl) were covered with <20 cm of unpacked snow and snow shielding was not applied.

3. Results and discussion

3.1. The assumption of steady state

We interpret the measured ^{10}Be concentrations in terms of average erosion rates to obtain an estimate of the magnitude of erosion and the pattern of erosion rates in the region. Therefore, it is important to evaluate how close isotopic concentrations are to steady state. When considering cosmogenic isotope concentrations in terms of erosion rates it is assumed that ^{10}Be concentrations represent constant, long-term (generally $>10^3$ years) erosion. Generally, this assumption is valid if: (1) a rock is eroded by a process that removes infinitely thin layers continuously, and (2) that a total thickness of at least 2 attenuation depths of fast neutrons has been eroded. This depth is dependent on the density of the matter being eroded. In our study area most of the rock being eroded is composed of granite and metasedimentary rocks, all of which have a density of 2.6–2.7 g cm^{-3} (Haeussler et al., 2017b). At such densities, the typical depth of attenuation would be ~60 cm (attenuation depth = Λ/ρ). At 2 attenuation depths (~120 cm) production decreases to $1/e^2$ of the surface production rate and the majority of cosmogenic nuclides are within that depth. In other words, once 120 cm of rock is removed by relatively constant erosion, ^{10}Be concentrations at the surface approach steady state (e.g. Kirchner et al., 2001; Glotzbach, 2015; Glotzbach et al., 2016).

We consider four geomorphic settings when discussing steady state:

1) Flat granitic surfaces on high parts of Denali. Here, particularly at the highest elevations, we observe the granodiorite erodes grain-by-grain and the resultant grus is slowly removed. Also, limited freeze-thaw (see subsequent section on meteorological observations) breaks down larger rock masses into crystal-size grains. These processes yield steady-state erosion. Furthermore, at these elevations and windswept locations, away from glacial cirques, glaciers do not override rock and there is no glacial erosion.
2) The cliffs of the upper glacial sidewalls. Erosion of the resistant granitic cliffs in the upper reaches of the Kahiltna Glacier, on the Kahiltna Peaks – a mountain on the east side of the glacier, occurs primarily by toppling, rockfall, and slab collapse, as well as by grain-by-grain erosion (as evidenced by the samples we collected on bedrock ledges). The concentration of ^{10}Be in sediment from this setting will depend on the thickness of the slabs and the frequency of slab detachment. Here, slabs that topple can be several meters in thickness, periodically exposing fresh rock faces that are not in isotopic steady state. Therefore, the erosion rates calculated from ^{10}Be concentrations measured in samples from the high granitic cliffs are maximum and must be considered cautiously (Reinhardt et al., 2007).
3) Slopes along the length of the glacier. For erosion rates between 100- and 600-mm per ka, typical of high and tectonically active mountain ranges (e.g. Scherler et al., 2014; Matmon et al., 2009, and references therein), 2–12 ka are required to remove 120 cm. This time span is shorter than the time since major post-Last Glacial Maximum deglaciation of the region. The threshold slope for the friable metasedimentary rocks that compose most of the slopes along the length of the glacier is ~20° (Ward et al., 2012), and erosion occurs through physical weathering of small grains and clast and shallow landslides. As long as these processes are dominant, ^{10}Be concentrations will reflect the actual long-term average erosion rate (Reinhardt et al., 2007). Therefore, at high erosion rates typical of tectonically active mountain ranges, such as the Alaska Range, we assume that at least 120 cm of rock have been eroded since deglaciation, and that ^{10}Be concentrations approach steady state. The approach to steady state, as opposed to the actual achievement of steady state, results in overestimated erosion rates and requires a correction. Glotzbach et al. (2014) model this correction and show that for deglaciation that occurred 10–15 ka and post-glaciation erosion rates that range between 100 and 600 mm/ka, corrected erosion rates remain at the hundreds of millimeters per thousand years magnitude.
4) Glacial outwash. Sediment from the entire glacial basin is mixed within the Kahiltna River. This includes sediment from the very high slopes, the headwalls of cirques, sediment from slopes along the glacier, and sediment eroded from the base of the glacier, which has not been exposed to cosmic radiation. Therefore, the assumption of steady state is problematic. Nevertheless, the very low ^{10}Be concentrations measured in all these samples indicate that erosion of slopes along the outwash river provide low-dosed ^{10}Be sediment to the river and erosion of the slopes must be operating at rates of 100 s of mm/ka.

Although we combine, and compare, several types of samples from different geomorphic settings in which different erosional processes influence their ^{10}Be concentrations, all samples provide an estimate of the rate of surface processes in their vicinity and can be interpreted broadly as indicating the rate of erosion.

3.2. Erosion at high elevations (3–5 km) on the Denali massif

^{10}Be concentrations in samples collected from granitic surfaces at high elevations of Denali ($n = 3$) are $948 \times 10^3 \pm 42 \times 10^3$ atoms g^{-1} quartz (3500 masl), $1628 \times 10^3 \pm 57 \times 10^3$ atoms g^{-1} quartz (4000 masl), and $17{,}593 \times 10^3 \pm 445 \times 10^3$ atoms g^{-1} quartz (5200 masl; Fig. 4 and Table 2). These concentrations are distinctively higher than those measured in the Kahiltna Peaks sidewall cliffs, Kahiltna Glacier moraine and Kahiltna River sediment samples. ^{10}Be concentrations of the three high-elevation samples show an increase with elevation. This increase is in part the result of the increase in cosmogenic nuclide production rate with elevation. However, this increase is apparent even after scaling these rates to sea level high latitude production rates, which results in erosion rate decrease with elevation. Erosion rates are calculated to 38.0 ± 5.0 mm/ka at 3500 masl, 28.6 ± 3.7 mm/ka at 4000 masl km, and 4.6 ± 0.6 mm/ka at 5200 masl (Fig. 4 and Table 2). These rates are similar to those measured on flat summits of the Appalachian Mountains (mean erosion rate 5.7 mm/ka ($n = 9$); Hancock and Kirwan, 2007) and on summits in several ranges in western North America (maximum mean erosion rate of 7.6 ± 3.9 mm/ka; Small et al., 1997). The similarity between erosion rates of summits of an ancient (Paleozoic) orogen (Appalachian Mountains), a Mesozoic-Cenozoic orogen (Rocky Mountains), and a presently active orogen (Alaska Range) is compelling given that their glacial history and current climates are vastly different. While these similarities may be spurious, it is possible that regardless of conditions (climate, rock type, and topography) all summits eventually approach steady-state erosion at relatively low rates. We follow Griffiths (1952), and *suggest that: "in this tectonically active part of the Alaska Range, where we would expect faster erosion, the nearly perpetual freezing conditions of the high summits contribute to the slow erosion rates" (Griffiths, 1952).*

3.3. Erosion on the sidewalls of the Kahiltna Glacier

The ^{10}Be concentrations on the sidewalls of the upper Kahiltna Glacier are one to two orders of magnitude lower than those measured on the higher surfaces (Fig. 4). ^{10}Be concentrations in samples collected from the Kahiltna Peaks ($n = 7$) range between $41.1 \times 10^3 \pm 4.0 \times 10^3$ and $140.4 \times 10^3 \pm 7.5 \times 10^3$ atoms g^{-1} quartz (Fig. 4 and Table 2) with an average of $78.8 \times 10^3 \pm 2.1 \times 10^3$ atoms g^{-1} quartz. Here, the granitic mountains erode in two major modes: 1) continuous surface erosion that produces sediment composed of sand and gravel. These particles contain the maximum possible concentration of cosmogenic nuclides and represent the continuous erosion of the exposed granitic surfaces, 2) toppling, rockfall, and slab collapse that produce massive piles of sediment composed of particles ranging in size from sand to boulders. The accumulation of cosmogenic nuclides in these particles ranges between the maximum possible to essentially zero. Sediment from both processes mix later in the medial moraine.

Each of the seven samples collected from the 500-m-tall sidewalls of the granitic Kahiltna Peaks near the head of the Kahiltna Glacier (above the ELA) represents a mix of grains that were detached from the exposed surface of the rock above the sample elevation. Measured concentrations in the seven samples collected from the granitic Kahiltna Peaks yielded erosion rates between 89 and 481 mm/ka, depending on the attributed shielding factor (Table 2; Matmon et al., 2020). Apart from one result, all calculations show high erosion rates, on the order of 10^2 mm/ka, typical for tectonically active regions of high mountainous relief (e.g. Matmon et al., 2009 and references therein; Matmon and Zilberman, 2017). These results show a dramatic increase in erosion rates as elevation decreases into the zone affected by glacial activity.

3.4. Medial moraine - upper glacier

The five samples collected from medial and lateral moraines at elevations that range between 1369 and 1394 masl yielded ^{10}Be concentrations between $8.9 \times 10^3 \pm 1.2 \times 10^3$ and $47.5 \times 10^3 \pm 5.0 \times 10^3$ atoms g^{-1} quartz (Fig. 4 and Table 2) with an average of $25.3 \times 10^3 \pm 2.6 \times 10^3$ atoms g^{-1} quartz. These concentrations are similar to those measured by Ward and Anderson (2011) on the medial moraines of glaciers in the nearby Kichatna Mountains.

^{10}Be concentration in the samples collected from medial moraines in the upper part of the glacier are distinctively and significantly lower than those measured from the sidewalls of the Kahiltna Glacier or from the high surfaces on Denali (Table 2 and Fig. 4). This indicates that sediment produced from high elevations, with high ^{10}Be concentrations, is not a significant component of the sedimentary volume in the medial moraines. Other sources, with much lower ^{10}Be concentrations, must supply the majority of the sediment to the medial moraine and dilute the concentration of sediment from the mountainsides. As discussed in Matmon et al. (2020), a major source for low-dosed sediment are the mountainside slopes adjacent to the medial moraines. These slopes less steep than those at higher terrains and are mostly underlain by softer low-grade metasedimentary rock. The generation of sediment from these slopes with a concentration of ~25,000 atoms g^{-1} quartz, which is the average ^{10}Be concentration of the five samples collected from medial moraines at the upper part of the glacier, requires erosion rates of about 300 mm/ka. The interpretation of the measured ^{10}Be concentrations in

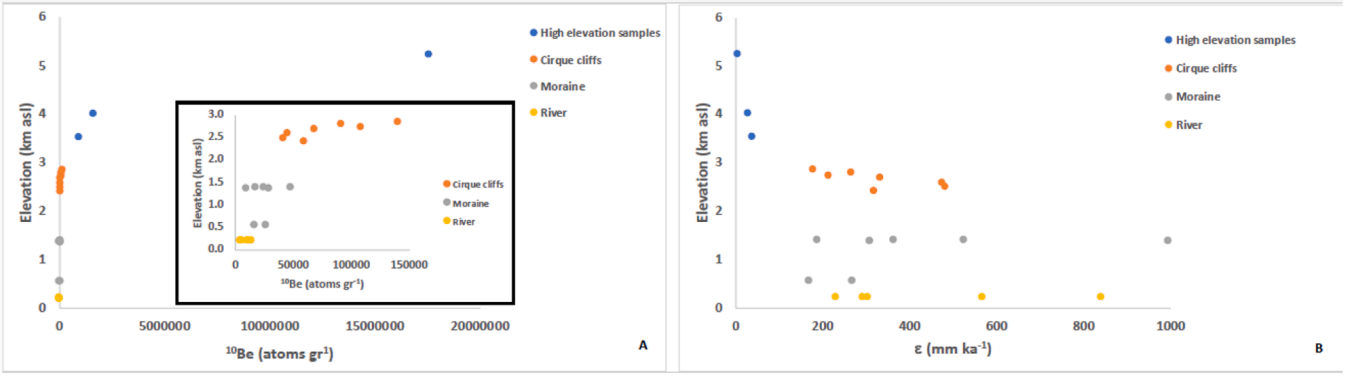


Fig. 4. Cosmogenic isotope results. A. ^{10}Be concentrations vs. elevation. Inset graph shows a close-up on the concentrations vs. elevation of all samples below 2.8 km. B. Steady state erosion rates (calculated from ^{10}Be concentrations) vs. elevation. Notice that although erosion rates in the cirque cliffs, medial moraines and alluvial samples are similar (100 s of mm/ka), the range of rates increases with the decrease in sample elevation.

Table 2
Laboratory data and erosion rates for Kahiltna basin samples.

Sample Name	Geomorphic location	Geographic location	Quartz (gr)	Be carrier (mg)	$^{10}Be/^{9}Be$ ($x10^{-15}$)	^{10}Be (10^3 atoms gr^{-1})	Scaling factor*	^{10}Be erosion rate (mm ka^{-1})*	Scaling factor**	^{10}Be erosion rate (mm ka^{-1})**	Scaling factor***	^{10}Be erosion rate (mm ka^{-1})***
Denali5242	Bedrock flat	High Denali slopes	10.052	0.2688	9844.23 ±152.46	17,593 ± 445	34.67	4.6 ± 0.6				
Denali4023	Bedrock flat	High Denali slopes	10.041	0.2604	939.03 ±26.66	1627.5 ± 56.5	19.17	28.6 ± 3.7				
Denali3535	Bedrock flat	High Denali slopes	10.014	0.2576	551.41 ±21.5	948.0 ± 41.5	14.65	38.0 ± 5.0				
14PH001	Cirque cliff	Kahiltna Peaks	12.221	0.18	142.61 ±7.06	140.38 ± 7.50	9.77	178.3 ± 23.9	4.90	89.0 ± 11.9	9.77	178.3 ± 23.9
14PH002	Cirque cliff	Kahiltna Peaks	12.362	0.266	63.39 ±3.42	91.16 ± 5.24	9.44	265.3 ± 35.9	4.73	132.5 ± 18.0	8.75	254.9 ± 33.3
14PH003	Cirque cliff	Kahiltna Peaks	10.984	0.2562	69.25 ±4.29	107.95 ± 7.02	9.03	214.1 ± 29.7	4.52	106.9 ± 14.9	7.73	193.3 ± 25.5
14PH004	Cirque cliff	Kahiltna Peaks	11.735	0.2646	44.91 ±3.15	67.67 ± 4.93	8.74	330.9 ± 47.2	4.38	165.3 ± 23.6	6.71	254.0 ± 36.2
14PH005	Cirque cliff	Kahiltna Peaks	14.144	0.2548	37.04 ±2.68	44.59 ± 3.35	8.24	473.7 ± 68.1	4.13	236.7 ± 34.0	5.69	326.9 ± 47.0
14PH006	Cirque cliff	Kahiltna Peaks	10.561	0.252	25.77 ±2.47	41.10 ± 4.02	7.71	481.0 ± 75.4	3.86	240.3 ± 37.7	4.67	291.1 ± 45.7
14PH007	Cirque cliff	Kahiltna Peaks	10.756	0.191	49.46 ±3.95	58.70 ± 4.83	7.30	318.5 ± 47.0	3.65	159.1 ± 23.5	3.65	159.1 ± 23.5
14PH017A	moraine	Kahiltna Glacier	8.909	0.2548	24.86 ±2.58	47.52 ± 5.03	3.47	187.0 ± 30.3				
14PH018A	moraine	Kahiltna Glacier	12.49	0.172	26.68 ±2.92	24.55 ± 2.73	3.48	363.4 ± 60.2				
14PH019A	moraine	Kahiltna Glacier	9.313	0.252	9.38 ±2.10	16.96 ± 3.82	3.47	524.5 ± 134.5				
14PH020A	moraine	Kahiltna Glacier	12.812	0.212	25.68 ±9.75	28.40 ± 10.79	3.42	308.0 ± 123.1				
14PH021A	moraine	Kahiltna Glacier	23.632	0.2618	12.20 ±1.59	8.88 ± 1.2	3.44	994.0 ± 180.0				
14PH023A	moraine	Kahiltna Glacier	11.013	0.17	25.48 ±3.48	26.29 ± 3.62	1.72	167.0 ± 30.9				
14PH024A	moraine	Kahiltna Glacier	11.267	0.2576	10.79 ±1.56	16.48 ± 2.41	1.73	268.7 ± 51.3				
14PH025	river	Kahiltna River	12.705	0.252	8.27 ±1.60	10.96 ± 2.13	1.24	290.7 ± 66.8				
14PH026	river	Kahiltna River	10.509	0.266	6.20 ±1.54	10.49 ± 2.62	1.24	303.6 ± 84.6				
14PH027	river	Kahiltna River	11.526	0.2772	2.36 ±1.26	3.79 ± 2.03	1.24	840.2 ± 460.6				
14PH028	river	Kahiltna River	14.179	0.2576	4.67 ±1.54	5.671.87	1.26	567.6 ± 200.0				
11PH013	river	Kahiltna River	18.782	0.212	18.50 ±3.20	13.96 ± 2.43	1.25	228.9 ± 48.8				

* Scaling factor for cirque cliff samples calculated assuming no shielding. Scaling factor for river samples considering sample elevation. Erosion rates calculated considering the corresponding scaling factors.
** Scaling factor for cirque cliff samples calculated assuming infinite vertical cliff. Erosion rates calculated considering the corresponding scaling factors.
*** Scaling factor for cirque cliff samples calculated assuming no shielding at the top most sample and linearly increasing the shielding to the lower most sample where an infinite vertical cliff is assumed.
#All calculations using a sea-level high-latitude production rate by spallation of 4.01 atoms/g/yr (Borchers et al., 2016).

terms of steady-state erosion of the adjacent slopes yields rates that range between 187±31 and 994±180 mm/ka (Table 2). These rates are rapid but reasonable for tectonically active mountainous regions with high relief (Matmon et al., 2009, and references therein), and especially with soft and friable underlying rock.

Furthermore, of the five samples collected and measured from the upper medial moraines, sample 14PH021 has the shortest distance to its source and it yielded the lowest ^{10}Be concentration of the five samples. As it was collected only 1 km downstream of its source area, the ^{10}Be concentration measured in sample 14PH021 ($8.9 \times 10^3 \pm 1.2 \times 10^3$ atoms g^{-1} quartz) reflects the erosion of the lowest-elevation slopes adjacent to the glacier. The rate of slope erosion required to supply sediment to the moraine with ^{10}Be concentration of ~9000 atoms g^{-1} quartz, similar to that measured in sample 14PH021, is nearly 1000 mm/ka. This result is consistent with our understanding that at low enough elevations (in the case of the Kahiltna Glacier, it is below 2800 m) under the erosional influence of the glacier, erosion rates increase dramatically relative to the high surfaces on Denali and the upper sidewalls of the Kahitna Glacier.

Overall, the majority of sediment supplied to the medial moraines is derived from two sources: 1) granitic peaks at the head of the Kahiltna Glacier that erode by the infrequent collapse of slabs and continuous erosion of the granitic surfaces, and 2) the lower slopes, around the ELA elevation, which erode at 100 s of millimeters per thousand years and supply material to lateral moraines that become medial moraines downslope. Regardless of the relative contribution of these two sources to the morainal material, ^{10}Be concentrations indicate both sources erode at 100 s of mm/ka.

3.5. Medial moraine - lower glacier

Similar erosion rates were obtained from the samples collected down

glacier (Fig. 4 and Table 2). The sedimentary cover on top of the ice increases and the supply of sediment from the slopes adjacent to the glacier is directly observed. The two medial moraine samples (14PH023 and 14PH024) from the lower glacier, collected at elevations of 551 and 559 masl, yielded ^{10}Be concentrations of $26.3 \times 10^3 \pm 3.6 \times 10^3$ and $16.5 \times 10^3 \pm 2.4 \times 10^3$ atoms g^{-1} quartz (Table 2). The average concentration in the moraine samples from the lower part of the glacier (14PH023–14PH024; $21.4 \times 10^3 \pm 2.2 \times 10^3$ atoms g^{-1} quartz) is somewhat less, but similar within error, to the average concentration of the moraine samples from the upper part of the glacier (samples 14PH017 to 14PH021; $25.3 \times 10^3 \pm 2.6 \times 10^3$ atoms g^{-1} quartz). This implies that sediment transport down glacier is rapid enough that there is insignificant accumulation of cosmogenic nuclides in exposed medial moraine material. If we use the Kahiltna Glacier velocity from near the ELA of ~300 m yr^{-1} (Goodwin et al., 2012), it would take ice 80–100 years to transit the 27 km from the location of the highest elevation medial moraine samples to the location of the lower medial moraine samples. This short transit time does not enable significant dosing. The slight decrease in ^{10}Be concentrations down glacier implies the addition of slope material that erodes faster than along the upper parts of the glacier and is dosed at a lower production rate (due to decreasing elevation). The additional material added to medial moraines from the nearby slopes must be added with a dose of ~20,000 atoms g^{-1} quartz. We calculate the range of erosion rates that would yield sediment with ^{10}Be concentration of 20,000 atoms g^{-1} quartz of the slopes adjacent to the path of the glacier. We consider the elevation of the high medial moraine samples (~1400 masl) and the elevation of the glacier terminus (~250 masl). We, therefore, estimate the erosion rates of the low-elevation slopes above the lower part of the glacier to range between 300 and 140 mm/ka. The interpretation of the measured ^{10}Be concentrations in terms of steady state erosion of the adjacent slopes yields rates that range between 167±31 and 269±51 mm/ka (Table 2). As in the case of the upper part of the glacier, slopes surrounding the glacier erode at rates of hundreds of millimeters per thousand years.

Ward et al. (2012) discuss the influence of rock type on glacial erosion. Their discussion is relevant to the subject of our paper in the underlying idea that friable and fractured rock (such as the metasedimentary rocks in the southern Alaska Range) erodes quickly, loses mass, and produces voluminous sediment, whereas resistant granitic rock erodes slowly, maintains steep cliffs and relief, and does not produce much sediment. They reached this conclusion through morphometric analyses of the glacial valley. We note that rocks exposed in their study area are the same rock units found along much of the Kahiltna Glacier. The difference in erodibility of the various rock types supports our interpretation that the majority of the sediment in the medial moraine is derived from the areas in the catchment that are underlain by metasedimentary rocks and not from the high granitic cliffs. We reach this same conclusion from a totally different dataset by comparing the high ^{10}Be concentrations measured in the granitic samples at high elevations relative to the low concentrations measured in the medial moraine material.

3.6. River sediment (downstream of the glacier terminus)

River sediment samples yield the lowest ^{10}Be concentrations among the four sample groups (Table 2). ^{10}Be concentrations in Kahiltna River sediment samples ($n = 5$; 14PH025–14PH028 and 11PH013) range between $5.7 \times 10^3 \pm 2.4 \times 10^3$ and $14 \times 10^3 \pm 2.4 \times 10^3$ atoms g^{-1} quartz (Table 2) with an average of $9 \times 10^3 \pm 1.0 \times 10^3$ atoms g^{-1} quartz. These values are lower than those measured in the medial moraines and indicate that medial moraine material must be mixed with low-dosed material from a different source. The possibilities for the source of such low-dosed material are the low elevation slopes on both sides of the Kahiltna River and material that was eroded from the base of the glacier. For material derived from slopes, we calculate the range of possible slope erosion rates by considering the elevation of the of the alluvial samples (~215 masl). If the low-dosed sediment was derived from these low-elevation slopes, erosion rates of the low-elevation slopes above the Kahiltna River would range between 230 and 840 mm/ka. If all material were to be derived from the base of the glacier, we assume that ^{10}Be concentrations would have approached zero.

3.7. Temperature, elevation, and freeze-thaw cycles

We consider the role of temperature on erosion processes at high elevations. We utilized meteorological data available at six elevations within the Kahiltna catchment along the West Buttress climbing route on Denali: 2130 masl (7000 feet – Denali 'base camp'), 3050 masl (10,017 ft), 4330 masl (14,200 ft – 'basin camp' or '14 camp'), 4940 masl (16,200 ft – 'top of the headwall'), and 5240 masl (17,200 feet – 'high camp'), and 5715 masl (18,750 feet – above 'Denali Pass'; Figs. 2,3 and 5). It is challenging to collect meteorological data from these locations, and the time series is discontinuous and variable between the five sites. Data for the 2130 masl (7000 ft) and 4330 masl (14,200 ft) sites are available from University of Utah Mesowest website (mesowest.utah.edu) and the data starts 31 May 2018 and extends to the present. The data from the 4940 masl (16,200 ft) and 5240 masl (17,200 ft) sites are from Yoshikawa (2014) and span about one year. The 4940 masl data start 11 July 2016 and end 30 June 2017. The 5240 masl data span from 29 June 2016 to 11 February 2017. Data for the 5715 masl (18,750 foot) site are from Hartl (2020b) and span much of the decade from 1990 to 2000 and then roughly 3 years of data between 2002 and 2006. The data show that the temperature rarely exceed freezing at 4330 masl (only briefly warming above freezing for 1 to several hours on 45 unique days out of 1132 day record at the 4330 masl camp), and it almost never (3 times in one year) exceeds freezing at 4940 masl. To underscore these observations, meteorological analysis of the NCEP–NCAR reanalysis 1 dataset (Kalnay et al., 2018) for the 1948–2018 period shows the temperature at the 500 hPa elevation (~5.5 km at mid latitudes), or near the summit of Denali is never above freezing (Hartl et al., 2020a).

3.8. Differential erosion and the growth of relief

Overall, the compilation of the above data shows that in the Denali massif-Kahiltna Glacier-Kahiltna River system, the highest elevation surfaces erode at 5–40 mm/ka. These slopes are almost entirely composed of resistant granitic rock and are almost always frozen (Figs. 2 and 5). At lower elevation, within a zone influenced by glacial activity, erosion increases dramatically to 100 s of mm/ka. This is true for: 1) the granitic sidewalls of the Kahiltna Glacier and may be explained by the steep topography, and the action of ice and snow on the cirque walls, and 2) for the gentler side slopes along the length of the glacier and the outwash river downstream from the glacier terminus. This may be explained by the friable bedrock and the intense freeze-thaw action at low elevations.

Of all cirque cliff, moraine, and alluvial samples, only one sample yielded an erosion rate lower than 100 mm/ka (sample 14PH001; scaling factor of 4.9; erosion rate = 89 mm/ka; Table 2). All other samples ($n = 18$) yielded erosion rates that ranges between 133 mm/ka and 994 mm/ka. All calculated rates are high and typical of tectonically active mountain ranges. As weathering and mass wasting along the mountain slopes is likely episodic and variable, we argue that the large range in calculated erosion rates does not reflect continuous processes. Rather, it is the result of the episodic nature of weathering and erosion in this landscape. Because these high erosion rates are averaged over a very short time (low 10^3 yrs) the calculated erosion rate of each sample may be controlled by specific mass-wasting events and change rapidly both in time and space. However, all results point to erosion operating at rates faster than 100 s of mm/ka (Fig. 4). In contrast, the samples from high elevations (3–5 km) all yielded erosion rates lower than 40 mm/ka.

Based on bedrock apatite fission-track data (Fitzgerald et al., 1995), rock uplift is occurring at a rate of 1.5 km/my, thus 1000 m of rock uplift

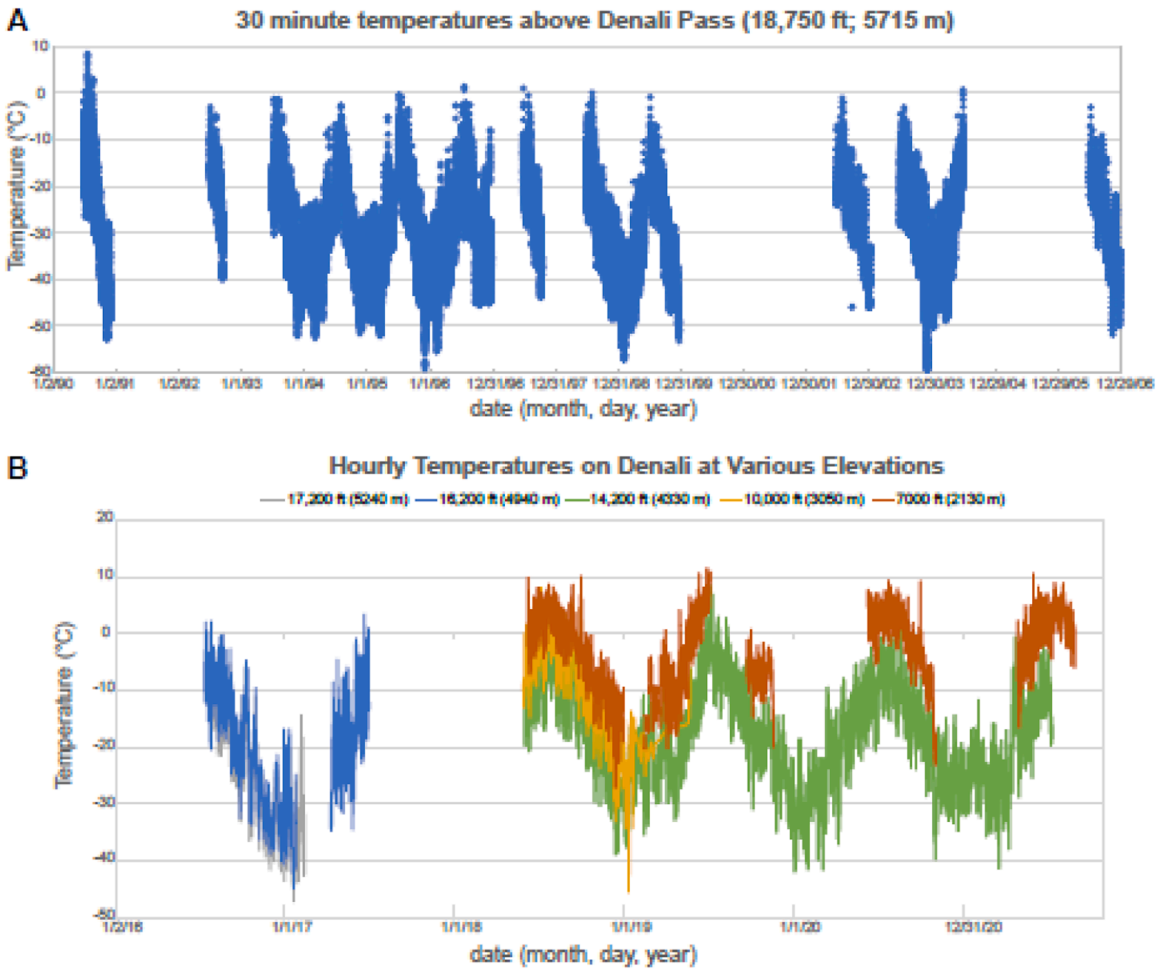


Fig. 5. Temperature data (in °C) at six elevations along the West Buttress climbing route: A. 5715 m (18,750 feet – 'Denali Pass'; Hartl, 2020). B. 2130 m (7000 feet – Denali 'base camp'; (mesowest.utah.edu)), 3050 m (10,017 feet), 4330 m (14,200 ft – 'basin camp' or '14 camp'; (mesowest.utah.edu), 4940 m (16,200 ft – 'top of the headwall'; Yoshikawa (2014), and 5240 m (17,200 feet – 'high camp'; Yoshikawa (2014). Data for the 2130 m (7000 ft) and 4330 m (14,200 ft) sites starts 31 May 2018 and extends to the present. The data from the 4940 m (16,200 ft) and 5240 m (17,200 ft) sites spans about one year. Data for the 18,750 foot site spans much of the decade from 1990 to 2000 and then roughly 3 years of data between 2002 and 2006. Overall, the data show that the temperature rarely exceeds freezing at 4330 m (the 14,200 foot camp), and it almost never (3 times in one year) exceeds freezing at 4940 m.

can occur in <700,000 yrs. However, a majority of this rock uplift is balanced by erosion in the lower parts of the drainage system such that surface uplift is minimal, while rock uplift and surface uplift in the higher parts of the drainage system are nearly equal due to very low erosion rates. Considering the difference in erosion rates between the high (5–38 mm ka^{-1}) and low (133–994 mm ka^{-1}) elevations, relief of 1000 m could be produced during a period of 1–10 Ma. This time range agrees well with an estimated increase in rock uplift and exhumation on Denali over the last ~6 Ma from thermochronology data (Fitzgerald et al., 1995).

Four factors combine along the southern side of the Alaska Range to result in high elevation, differential erosion, and an increase of relief over time: 1) Tectonics. Without the active Denali fault system advecting rock into and through a restraining bend, high topography would not exist. However, if tectonics were the only factor in producing topography, we would expect a gradual rise in topography from the lower mountains of the Alaska Range to the highest elevations and back down again, as rocks are moved through the bend in the fault system. Anderson (1990) showed this for the Santa Cruz Mountains of California traveling through a bend in the San Andreas system. Also, Lease et al. (2016) demonstrated from detrital thermochronology that rocks are transported through the bend in the Denali fault system, and that the bend's location is fixed. Benowitz et al. (2021) reached the same conclusion based on physical models. 2) Rock type. The high elevation slopes are composed of resistant granodiorite, with a low fracture density, steep slopes, and presumably a high rock strength. In contrast, lower elevation slopes are underlain by highly fractured metasedimentary rock, with high fracture density, lower slopes, and a lower rock strength. 3) High elevation climate versus low elevation climate. Our ^{10}Be data show that erosion rates above 3000 m are significantly slower than below 3000 m. This is consistent with the meterological data showing that it is uncommon to be above freezing at 4330 m. Rock weathering processes - particularly frost-cracking - are controlled by temperature (e.g. Walder and Hallet, 1985, 1986). Anderson (1998), using empirical data, found the 'frost-cracking window' lies between −3° and −8 °C, which promotes higher porosity, growth of ice lenses, and thus rock damage. Rempel et al. (2016) showed both the decreasing effects of frost-cracking with depth in bedrock at lower mean-annual temperatures (MAT), but also showed that larger MAT amplitude increases frost cracking. Nonetheless, at high elevations on Denali, temperatures below the frost-cracking window prevail and thus frost cracking has limited efficiency, whereas at lower elevations frost weathering can occur vigorously.

Glaciers are also far more erosive at lower and warmer elevations. Griffiths (1952) noted the lack of high-elevation cirques above 16,000 ft (or 4877 m), which argues for little glacial erosion high on the

mountain. At lower elevations, the action of glacial activity, starting with the erosion in the glacial cirque through the abrasive power of the glacier while it flows down valley, promote erosion along the margins of the glacier. Our ^{10}Be data indicate erosion rates between 175 and 1000 mm/ka, consistent with rapid erosion where glaciers slide at their base and can remove material. 4) Morphology. Steep morphology of the cirque walls promotes slab detachment and increased weathering. In the Kahiltna catchment, these factors combine in a way that amplifies differential erosion and increases relief. Given the combination of the active tectonic driver of the Denali fault that advects material into the bend of the fault system with extremely low erosion rates (controlled by high rock strength and continuous temperatures below the frost-cracking window), results in the disproportionately high topography and relief of Denali, and the adjacent peaks of Mounts Foraker and Hunter.

The high Himalayan mountains are another place on Earth where it is perennially below freezing, where there is reduced erosion, and where there is a tectonic driver for topography to continue to grow. Lavé et al. (2023) recently found evidence for a 23 km^3 landslide in 1190 CE from the Annapurna massif, which was sourced from a paleosummit of the 8000+ *m* mountain. They speculated that, *"…once a mountain peak passes over the zone in which rock mass is permanently frozen and the intensity of frost cracking decreases substantially, the frozen conditions provide enhanced protection against surface erosion. This may even initiate a positive feedback…"*(Lave et al., 2023, pg. 100). This idea is supported by our ^{10}Be data from Denali. Their study also portends that megalandslides are the only possible mechanism for reducing topography of summits that become too high since "normal" erosion does not operate at these high elevations.

4. Conclusions

We combined new and previously published ^{10}Be concentrations to form a 5000-meter elevation transect that shows an inverse relationship between erosion rates and elevation. This inverse relationship promotes the growth of relief with time. The samples that were analyzed include: 1) three new gravel samples between 3500 and 5200 masl from sites unaffected by recent glacial erosion, 2) previously published samples from a sidewall of the Kahiltna Glacier from 2400 to 2800 masl, 3) previously published samples from medial moraines along the length of the Kahiltna Glacier, from ~500 to 1400 masl, and 4) previously published alluvial samples along the Kahiltna River at an elevation of ~200 masl. Erosion rates for the three new high-elevation samples are remarkably low (~5–40 mm/ka) and are 1–2 orders of magnitude slower than those measured on cliffs around the glacial cirque, on medial moraines, and in river sediments below the glacier. Meteorological data from high elevations on Denali show that temperature rarely exceeds freezing above 4300 masl, indicating that frost weathering plays a minimal role in erosion at the highest elevations.

The differences in erosion rates can create relief of 1 km within 1–10 Ma, well within the estimated period of increase in rock uplift on Denali over the last ~6 Ma. The low ^{10}Be concentrations of low elevation samples from the Kahiltna Glacier and Kahiltna River show that high-elevation erosion is a negligible contributor to the overall sediment budget of the catchment. These data from Denali show the combined influence of climate (manifested by glacial erosion above vs. below glacial cirques, and by freeze-thaw cycles), rock strength, and topography on the development of relief in a tectonically active mountain range.

CRediT authorship contribution statement

A. Matmon: Writing – review & editing, Writing – original draft, Conceptualization. **P.J. Haeussler:** Writing – review & editing, Writing – original draft, Funding acquisition. **M. Loso:** Data curation.

Declaration of competing interest

The authors declare that they have no known competing financial interests or personal relationships that could have appeared to influence the work reported in this paper.

Data availability

All Data used is presented in Tables 1 and 2 and in Matmon et al., 2020

Acknowledgements

Thanks to Kara Haeussler and Abby Gahm for help in collecting the high elevation samples.

References

Anderson, R.S., 1998. Near-surface thermal profiles in alpine bedrock: implications for the frost weathering of rock. Arct. Alp. Res. 30 (4), 362–372.
Anderson, R.S., 1990. Evolution of the northern Santa Cruz Mountains by advection of crust past a San Andreas fault bend. Science 249 (4967), 397–401.
Avouac, J.P., Burov, E.B., 1996. Erosion as a driving mechanism of intracontinental mountain growth. J. Geophys. Res.: Solid Earth 101 (B8), 17747–17769.
Balco, G., Stone, J.O., Lifton, N.A., Dunai, T.J., 2008. A complete and easily accessible means of calculating surface exposure ages or erosion rates from 10Be and 26Al measurements. Quat. Geochronol. 3 (3), 174–195.
Benowitz, J.A., Cooke, M.L., Terhune, P.J., Herreid, S., Bemis, S.P., Toeneboehn, K., Waldien, T.S., O'Sullivan, P.B., 2021. Why is denali (6,194 m) so big? Caught inside the tectonic wake of a migrating restraining bend. Terra Nova 1–14. https://doi.org/10.1111/ter.12571.
Bierman, P.R., 1994. Using in situ produced cosmogenic isotopes to estimate rates of landscape evolution: a review from the geomorphic perspective. J. Geophys. Res.: Solid Earth 99 (B7), 13885–13896.
Bierman, P.R., Caffee, M.W., 2001. Slow rates of rock surface erosion and sediment production across the Namib Desert and escarpment, southern Africa. Am. J. Sci. 301, 326–358. https://doi.org/10.2475/ajs.301.4-5.326.
Boulton, G.S., 1972. The role of thermal regime in glacial sedimenta- tion. In: Price, R.J., Sugden, D.E. (Eds.), Polar Geomorphology. IBG Special Publication, pp. 1–19.
Borchers, B., Marrero, S., Balco, G., Caffee, M., Goehring, B., Lifton, N., Nishiizumi, K., Phillips, F., Schaefer, J., Stone, J., 2016. Geological calibration of spallation production rates in the CRONUS Earth project. Quat. Geochronol. 31, 188–198. https://doi.org/10.1016/j.quageo.2015.01.009.
Boulton, G.S., 1974. Processes and patterns of glacial erosion. In: Glacial Geomorphology: A proceedings volume of the Fifth Annual Geomorphology Symposia Series, held at Binghamton New York September 26–28, 1974. Dordrecht. Springer Netherlands, pp. 41–87.
Brocklehurst, S.H., Whipple, K.X., 2002. Glacial erosion and relief production in the Eastern Sierra Nevada, California. Geomorphology 42 (1–2), 1–24.
Brocklehurst, S.H., Whipple, K.X., Foster, D., 2008. Ice thickness and topographic relief in glaciated landscapes of the western USA. Geomorphology 97, 35–51. https://doi.org/10.1016/j.geomorph.2007.02.037.
Brozović, N., Burbank, D.W., Meigs, A.J., 1997. Climatic limits on landscape development in the northwestern Himalaya. Science 276, 571–574. https://doi.org/10.1126/science.276.5312.571.
Burkett, C.A., Bemis, S.P., Benowitz, J.A., 2016. Along-fault migration of the Mount McKinley restraining bend of the Denali fault defined by late Quaternary fault patterns and seismicity, Denali National Park & Preserve, Alaska. Tectonophysics 693, 489–506.
Dethier, D.P., Ouimet, W., Bierman, P.R., Rood, D.H., Balco, G., 2014. Basins and bedrock: spatial variation in 10Be erosion rates and increasing relief in the southern Rocky Mountains, USA. Geology 42 (2), 167–170.
Eberhart-Phillips, D., Haeussler, P.J., Freymueller, J.T., Frankel, A.D., Rubin, C.M., Craw, P., Ratchkovski, N.A., Anderson, G., Carver, G.A., Crone, A.J., Dawson, T.E., 2003. The 2002 Denali fault earthquake, Alaska: a large magnitude, slip-partitioned event. Science 300 (5622), 1113–1118.
Fitzgerald, P.G., Stump, E., Redfield, T.F., 1993. Late Cenozoic uplift of Denali and its relation to relative plate motion and fault morphology. Science 259, 497–499.
Fitzgerald, P.G., Sorkhabi, R.B., Redfield, T.F., Stump, E., 1995. Uplift and denudation of the central Alaska Range: a case study in the use of apatite fission track thermochronology to determine absolute uplift parameters. J. Geophys. Res.: Solid Earth 100 (B10), 20175–20191. https://doi.org/10.1029/95JB02150.
Glotzbach, C., 2015. Deriving rock uplift histories from data-driven inversion of river profiles. Geology 43 (6), 467–470.
Glotzbach, C., Paape, A., Baade, J., Reinwarth, B., Rowntree, K., Miller, J., 2016. Cenozoic landscape evolution of the Kruger National Park as derived from cosmogenic nuclide analyses. Terra Nova 28 (5), 316–322.

Glotzbach, C., Rottjer, M., Hampel, A., Hetzel, R., Kubik, P.W., 2014. Quantifying the impcat of former glaciationon catchment-wide denudation ratesderived from cosmogenic 10Be. Terra Nova 26 (3), 186–194.
Goodwin, K., Loso, M.G., Braun, M., 2012. Glacial transport of human waste and survival of fecal bacteria on Mt. McKinley's Kahiltna Glacier, Denali National Park, Alaska. Arct. Antarct. Alp. Res. 44 (4), 432–445. http://www.bioone.org/doi/full/10.1657/1938-4246-44.4.432.
Granger, D.E., Muzikar, P.F., 2001. Dating sediment burial with in situ–produced cosmogenic nuclides: theory, techniques, and limitations. Earth Planet. Sci. Lett. 188, 269–281. https://doi.org/10.1016/S0012-821X(01)00309-0.
Granger, D.E., Smith, A.L., 2000. Dating buried sediments using radioactive decay and muogenic production of 26Al and 10Be. Nuclear Instruments & Methods in Physics Research, Section B, Beam Interactions with Materials and Atoms 172, 822–826. https://doi.org/10.1016/S0168-583X(00)00087-2.
Griffiths, T.M., 1952. Glacial geomorphology on the Mt. McKinley massif, Alaska. In: Proceedings, Eighth General Assembly and Seventeenth International Congress. Washington, D.C.. International Geographical Union, pp. 331–336.
Haeussler, P.J., 2008. An overview of the neotectonics of interior Alaska: far-field deformation from the Yakutat microplate collision, in: Freymueller, J.T., Haeussler, P.J., Wesson, R.J., Ekstrom, G. (Eds.): Active Tectonics and Seismic Potential of Alaska. Geophysical Monograph Series 179, pp. 269–285.
Haeussler, P.J., Matmon, A., Schwartz, D.P., Seitz, G.G., 2017a. Neotectonics of interior Alaska and the late quaternary slip rate along the denali fault system. Geosphere 13, 1445–1463. https://doi.org/10.1130/GES01447.1.
Haeussler, P.J., Saltus, R.W., Stanley, R.G., Ruppert, N., Lewis, K., Karl, S.M., Bender, A., 2017b. The peters hills basin, a Neogene wedge-top basin on the Broad Pass thrust fault, south-central Alaska. Geosphere 13, 1464–1488. https://doi.org/10.1130/GES01487.1.
Hallet, B., 1981. Glacial abrasion and sliding: their dependence on the debris concentration in basal ice. Ann. Glaciol. 2, 23–28.
Hampton, B.A., Ridgway, K.D., Gehrels, G.E., 2010. A detrital record of Mesozoic island arc accretion and exhumation in the North American cordillera: u-Pb geochronology of the Kahiltna basin, southern Alaska. Tectonics 29, TC4015. https://doi.org/10.1029/2009TC002544.
Hancock, G., Kirwan, M., 2007. Summit erosion rates deduced from 10Be: implications for relief production in the central Appalachians. Geology 35 (1), 89–92.
Herman, F., Beyssac, O., Brughelli, M., Lane, S.N., Leprince, S., Adatte, T., Lin, J.Y., Avouac, J.P., Cox, S.C., 2015. Erosion by an Alpine glacier. Science 350 (6257), 193–195.
Hung, C.-H., 2008. Zircon U-Pb Ages and Geochemical Characteristics of the McKinley Sequence and Associated plutons, Central Alaska Range. National Taiwan University, Taipei.
Hurst, M.D., Mudd, S.M., Attal, M., Hilley, G., 2013a. Hillslopes record the growth and decay of landscapes. Science 341 (6148), 868–871.
Hartl, L., Stuefer, M., Saito, T., 2020a. The mountain weather and climate of Denali, Alaska—An overview. J. Appl. Meteorol. Climatol. 59 (4), 621–636.
Hartl, L., Stuefer, M., Saito, T., Okura, Y., 2020b. History and Data Records of the Automatic Weather Station on Denali Pass (5715 m), 1990–2007. J. Appl. Meteorol0. Climatol. 59 (12), 2113–2127.
Kalnay, E., Kanamitsu, M., Kistler, R., Collins, W., Deaven, D., Gandin, L., Iredell, M., Saha, S., White, G., Woollen, J., Zhu, Y., 2018. The NCEP/NCAR 40-year reanalysis project. Renewable Energy (pp. Vol1_146-Vol1_194). Routledge.
Kirchner, J.W., Finkel, R.C., Riebe, C.S., Granger, D.E., Clayton, J.L., King, J.G., Megahan, W.F., 2001. Mountain erosion over 10 yr, 10 k.y., and 10 m.y. time scales. Geology 29 (7), 591–594.
Kohl, C.P., Nishiizumi, K., 1992. Chemical isolation of quartz for measurement of in-situ–produced cosmogenic nuclides. Geochim. Cosmochim. Acta 56, 3583–3587. https://doi.org/10.1016/0016-7037(92)90401-4.
Lal, D., 1991. Cosmic ray labeling of erosion surfaces: in situ production rates and erosion models. Earth Planet. Sci. Lett. 104, 424–439. https://doi.org/10.1016/0012-821X(91)90220-C.
Lave, J., Guerin, C., Valla, P.G., Guillou, V., Rigaudier, T., Benedetti, L., France-Lanord, c., Gajurel, A.P., Morin, G., Duumoulin, J.P., Moreau, C., 2023. Medievel demise of a Himalayan giant summit induced by mega-landslide. Nature 619 (7968), 94–101.
Lease, R.O., 2018. Pliocene erosional pulse and glacier-landscape feedbacks in the western Alaska Range. Earth Planet. Sci. Lett. 497, 62–68. https://doi.org/10.1016/j.epsl.2018.06.009.
Lease, R.O., Haeussler, P.J., O'Sullivan, P., 2016. Changing exhumation patterns during Cenozoic growth and glaciation of the Alaska Range: insights from detrital thermochronology and geochronology. Tectonics 35 (4), 934–955. https://doi.org/10.1002/2015TC004067.
Loso, M.G., 2022. Glacier monitoring in Denali and Wrangell-St. Elias National Park and Preserve, 2016-2021: inventory and Monitoring Program, Central Alaska Network. Monitoring Summary Report. National Park Service, Copper Center AK.
Matmon, A., Haeussler, P.J., ASTER Team, 2020. Sediment sources and transport by the Kahiltna Glacier and other catchments along the south side of the Alaska Range, Alaska. Geosphere 16. https://doi.org/10.1130/GES02190.1.
Matmon, A., Bierman, P., Larsen, J., Southworth, S., Pavich, M., Caffee, M., 2003. Erosion of an ancient mountain range, the Great smoky mountains, North Carolina and Tennessee. Am. J. Sci. 303, 817–855.
Matmon, A., Simhai, O., Amit, R., Haviv, I., Porat, N., McDonald, E., Benedetti, L., Finkel, R., 2009. Where erosion ceases: desert pavement coated surfaces in extreme deserts present the longest-lived landforms on Earth. Geol. Soc. Am. Bull. 121, 688–697. https://doi.org/10.1130/B26422.1.
Matmon, A., Zilberman, E., 2017. Landscape evolution along the Dead Sea fault and its margins. In: Enzel, Y., Bar-Yosef, O. (Eds.), The Quaternary of the Levant. Cambridge University Press, Cambridge, UK, pp. 17–30. https://doi.org/10.1017/9781316106754.003.
Montgomery, D.R., 1994. Valley incision and the uplift of mountain peaks. J. Geophys. Res.: Solid Earth 99 (B7), 13913–13921.
Mitchell, S.G., Montgomery, D.R., 2006. Influence of a glacial buzz- saw on the height and morphology of the Cascade Range in central Washington State, USA. Quat. Res. 65, 96–107. https://doi.org/10.1016/j.yqres.2005.08.018.
Plafker, G., Naeser, C.W., Zimmerman, R.A., Lull, J.S., Hudson, T., 1992. Cenozoic uplift history of the Mount McKinley area in the central Alaska Range based on fission-track dating. In: Bradley, D.C., Dusel-Bacon, C. (Eds.), Geologic studies in Alaska by the U.S. Geological Survey, 1991, U.S. Geol. Surv. Bull. 2041, pp. 202–212.
Portenga, E.W., and Bierman, P.R., 2011. Understanding Earth's eroding surface with 10Be.
Quigley, M., Sandiford, M., Fifield, K., Alimanovic, A., 2007. Bedrock erosion and relief production in the northern Flinders Ranges, Australia. Earth Surface Processes and Landforms: The Journal of the British Geomorphological Research Group 32 (6), 929–944.
Reed, B.L., and Nelson, S.W., 1980, Geologic Map of the Talkeetna Quadrangle: U.S. Geological Survey Miscellaneous Field Investigations Map I-1174, 1 sheet, and 24 p., scale 1:250,000. /10 .1002 /esp .1415.
Reed, B.L., Lanphere, M.A., 1973. Alaska-Aleutian Range batholith: geochronology, chemistry, and relation to circum-Pacific plutonism. Geol. Soc. Am. Bull. 84 (8), 2583–2610. https://doi.org/10.1130/00167606(1973)84<2583:ARBGCA>2.0.CO;2.
Reinhardt, L.J., Hoey, T.B., Barrows, T.T., Dempster, T.J., Bishop, P., Fifield, L.K., 2007. Interpreting erosion rates from cosmogenic radionuclide concentrations measured in rapidly eroding terrain. Earth Surf. Processes Landforms 32, 390–406.
Regan, S.P., Benowitz, J.A., Holland, M.E., 2020. A plutonic brother from another magma mother: disproving the Eocene Foraker- McGonagall pluton piercing point and implications for long term slip on the Denali fault. Terra Nova 32, 66–74. https://doi.org/10.1111/ter.12437.
Rempel, A.W., Marshall, J.A., Roering, J.J., 2016. Modeling relative frost weathering rates at geomorphic scales. Earth Planet. Sci. Lett. 453, 87–95.
Riebe, C.S., Kirchner, J.W., Finkel, R.C., 2003. Long-term rates of chemical weathering and physical erosion from cosmogenic nuclides and geochemical mass balance. Geochim. Cosmochim. Acta 67 (22), 4411–4427.
Scherler, D., Bookhagen, B., Strecker, M.R., 2014. Tectonic control on 10Be-derived erosion rates in the Garhwal Himalaya, India. J. Geophys. Res. 119 (2), 83–105. https://doi.org/10.1002/2013JF002955.
Small, E.E., 1995. Hypsometric forcing of stagnant ice margins: pleistocene valley glaciers, San Juan Mountains, Colorado. Geomorphology 14 (2), 109–121.
Small, E.E., Anderson, R.S., Repka, J.L., Finkel, R., 1997. Erosion rates of alpine bedrock summit surfaces deduced from in situ 10Be and 26Al. Earth Planet. Sci. Lett. 150 (3–4), 413–425.
Small, E.E., Anderson, R.S., 1998. Pleistocene relief production in Laramide mountain ranges, western United States. Geology 26 (2), 123–126.
Stone, J.O., 2000. Air pressure and cosmogenic isotope production. J. Geophys. Res. 105, 23753–23759. https://doi.org/10.1029/2000JB900181.
Ward, D.J., Anderson, R.S., Haeussler, P.J., 2012. Scaling the Teflon Peaks: rock type and the generation of extreme relief in the glaciated western Alaska Range. J. Geophys. Res. 117, F01031. https://doi.org/10.1029/2011JF002068.
Walder, J., Hallet, B., 1985. A theoretical model of the fracture of rock during freezing. Geol. Soc. Am. Bull. 96, 336–346.
Walder, J., Hallet, B., 1986. The physical basis of frost weathering: toward a more fundamental and unified perspective. Arct. Alp. Res. 18, 27–32.
Ward, D.L., Anderson, R.S., 2011. The use of ablation-dominated medial moraines as samplers for 10Be-derived erosion rates of glacier valley walls, Kichatna Mountains, AK. Earth Surf. Processes Landforms 36, 495–512. https://doi.org/10.1002/esp.2068.
Whipple, K.X., Kirby, E., Brocklehurst, S.H., 1999. Geomorphic limits to climate-induced increases in topographic relief. Nature 401, 39–43. https://doi.org/10.1038/43375.
Whittaker, A.C., 2012. How do landscapes record tectonics and climate? Lithosphere 4 (2), 160–164. https://doi.org/10.1130/RF.L003.1.
Yoshikawa, K., 2014. Unpublished raw data from two high elevation weather stations on Denali. Data processing by Kenneth Hill, National Park Service. Work from research permit #957 titled: climatic history and jet stream variability analysis from Denali Automatic Weather Stations. University of Alaska Fairbanks.
Zeitler, P.K., Meltzer, A.S., Koons, P.O., Craw, D., Hallet, B., Chamberlain, C.P., Kidd, W. S., Park, S.K., Seeber, L., Bishop, M., Shroder, J., 2001. Erosion, Himalayan geodynamics, and the geomorphology of metamorphism. GSA Today 11 (1), 4–9.

Further reading

Hurst, M.D., Mudd, S.M., Attal, M., Hilley, G., 2013b. Hillslopes record the growth and decay of landscapes. Science 341 (6148), 868–871.